Atmos. Chem. Phys. Discuss., 12, 15373–15417, 2012
www.atmos-chem-phys-discuss.net/12/15373/2012/
doi:10.5194/acpd-12-15373-2012

Atmospheric Chemistry and Physics Discussions

No statistically significant effect of a short-term decrease in the nucleation rate on atmospheric aerosols

E. M. Dunne, L. A. Lee, C. L. Reddington, and K. S. Carslaw

School of Earth and Environment, University of Leeds, Leeds, UK

Received: 11 May 2012 – Accepted: 29 May 2012 – Published: 18 June 2012

Correspondence to: E. M. Dunne (e.dunne@leeds.ac.uk)

Published by Copernicus Publications on behalf of the European Geosciences Union.

Abstract

Observed correlations between short-term decreases in cosmic ray ionisation and cloud and aerosol properties have been attributed to short-term decreases in the ion-induced nucleation rate. We use a global aerosol microphysics model to determine whether a 10-day reduction of 15 % in the nucleation rate could generate a statistically significant response in aerosol concentrations and optical properties. As an upper limit to the possible effect of changes in the ion-induced nucleation rate, we perturb the total nucleation rate, which has been shown to generate particle concentrations and nucleation events in reasonable agreement with global observations. When measured against a known aerosol control state, the model predicts a 0.15 % decrease in global mean cloud condensation nucleus concentrations at the surface. However, taking into account the variability in aerosol, no statistically significant response can be detected in concentrations of particles with diameters larger than 10 nm, in cloud condensation nuclei with diameters larger than 70 nm, or in the Ångström exponent. The results suggest that the observed correlation between short-term decreases in cosmic ray ionisation and cloud and aerosol properties cannot be explained by associated changes in the large-scale nucleation rate.

1 Introduction

A link between galactic cosmic rays (GCRs) and the Earth's climate has been observed in multiple data sets over a range of timescales (Svensmark and Friis-Christensen, 1997; Bond et al., 2001; Neff et al., 2001; Kirkby, 2007; Eichler et al., 2009). However, the cause of this correlation has not yet been identified.

GCRs are made up of highly energetic charged particles which travel through the interstellar medium and impact on the Earth's atmosphere. GCRs create ions pairs when they collide with air molecules, and are the main source of atmospheric ions throughout the free troposphere and an important source in the boundary layer, where

ACPD
12, 15373–15417, 2012

radon decay also creates ions (Zhang et al., 2011). The GCR flux is controlled in part by the sun's magnetic activity, leading to variations in flux on timescales of a few days to millennia (Usoskin et al., 2005).

It is not known whether GCRs affect the climate directly through changes in atmospheric composition (such as aerosol and cloud properties) or whether they are a proxy for another climate-influencing factor. Changes in total solar irradiance over the solar cycle (0.036 % between solar cycles 21 and 22, Willson, 1997) are much smaller than would be necessary to account for the observed correlations, but changes in the UV portion of the solar spectrum are larger and may affect stratospheric heating, ozone concentrations and the atmospheric general circulation (Haigh, 1996; Haigh et al., 2010).

Two mechanisms have been proposed to account for the observed correlations between GCR flux and the climate: the ion-aerosol clear-air effect and the ion-aerosol near-cloud effect (Carslaw et al., 2002). The ion-aerosol near-cloud effect (Tinsley et al., 2000; Harrison, 2008; Harrison et al., 2011) refers to the effects on cloud microphysical properties caused by the accumulation of space charge on the top of clouds. Unipolar space charge accumulates due to the electric current flowing into the cloud from the fair-weather electric circuit. It is hypothesised that modulation of the fair-weather current by variations in cosmic ray ionisation could lead to a sequence of micro- and macrophysical responses in clouds. Aerosol particles and cloud droplets in this charged region can accumulate large charges of up to 1500 e on individual droplets (Twomey, 1956; Beard et al., 2004), possibly affecting aerosol particle activation (Harrison and Ambaum, 2008), scavenging processes (Wang et al., 1978; Tripathi and Harrison, 2002) and ice nucleation (Tinsley et al., 2000).

In the ion-aerosol clear-air effect, it is hypothesised that changes in the ionisation rate affect the formation of cloud condensation nuclei (CCN), which leads to changes in cloud drop concentrations, cloud albedo and other properties. Several model studies, including Pierce and Adams (2009b), Merikanto et al. (2009) and Yu and Luo (2009), have shown that nucleation in the free troposphere and boundary layer is an important

ACPD
12, 15373–15417, 2012

source of global tropospheric CCN, contributing between 23 and 70 % of all CCN (with the remainder from primary particle emissions). It is hypothesised that if some of these CCN are created through ion-induced nucleation then global CCN could be influenced by the cosmic ray ionisation rate. The nucleation rate has been shown experimentally to increase with ion concentrations (Kirkby et al., 2011; Enghoff et al., 2011). Pierce and Adams (2009a) found that the effect of changes in cosmic rays over a solar cycle on CCN concentrations would be two orders of magnitude too small to account for observed changes in cloud properties. In a global model study, Yu and Luo (2009) found that ion-mediated nucleation could generate a global aerosol field in good agreement with atmospheric measurements of CCN at 0.4 % supersaturation. Kazil et al. (2012) investigated the sensitivity of the atmosphere to changes in the ion-induced nucleation rate over a solar cycle, but found a negligible response.

Even though nucleation is an important source of CCN, Merikanto et al. (2009) found that a decrease in either the free tropospheric or boundary layer nucleation rate would not result in a proportionate decrease in CCN. A very large fraction of freshly nucleated particles are lost to the coagulation sink of pre-existing particles, and the proportion of nucleated particles which grow to CCN sizes is so small, that the response is strongly damped. Pierce and Adams (2007) estimated that an average of between 1 and 40 % of nucleated particles go on to form CCN. These studies suggest that large scale changes in nucleation rate would need to be very substantial to have any impact on global CCN and clouds.

Attribution of changes in cloud properties to changes in GCR flux over the solar cycle (Svensmark and Friis-Christensen, 1997) is hampered because variations in the solar radiation flux may also cause changes in climate variables. To overcome this difficulty, transient decreases in GCR flux on the timescale of a few days have been used instead. During periods of intense solar magnetic activity, streams of coronal matter ejected from the sun can block incoming GCRs. The resulting transient reduction in cosmic ray intensity is known as a Forbush decrease (Forbush, 1946). These

ACPD
12, 15373–15417, 2012

short-term decreases in GCR flux, which do not correlate with solar irradiance, have been used to test the GCR-climate connection.

One of the earliest studies of the correlation between Forbush decreases and cloud cover was carried out by Pudovkin and Veretenenko (1995). They examined measurements of clear and cloudy skies from observatories in the USSR. The observatories were divided into three groups based on latitude: $\phi \approx 50^{\circ}$ N, $\phi \approx$60–64° N, and $\phi \approx$ 65–68° N. They found a decrease in total cloud cover in the two northernmost latitude bands following winter-time Forbush decreases. In the latitudinal belt $\phi \approx$60–64° N, on the days immediately following winter-time Forbush decreases, the sky was more likely to be clear and less likely to be cloudy at noon.

Svensmark et al. (2009) observed a correlation between a selection of five Forbush decreases and four separate data sets of cloud and aerosol properties. They examined the Ångström exponent at 340–440 nm ($AE_{340-440}$) as measured by AERONET, the cloud water content measured by the Special Sensor Microwave/Imager (SSM/I), liquid water cloud fraction measured by the Moderate Resolution Imaging Spectroradiometer (MODIS), and low IR-detected clouds compiled by the International Satellite Cloud Climatology Project (ISCCP). These data sets were compared with neutron counts from CLIMAX, Colorado. They found minima in each of the data sets after lags of between 4 and 10 days from the minimum of the Forbush decrease and concluded that the minima were likely to be due to short-term changes in the ion-induced nucleation rate.

The findings of Svensmark et al. (2009) have been questioned and the relevant data sets re-examined in several papers. Laken et al. (2009) examined the MODIS liquid water cloud fraction data for evidence of a decrease following Forbush decreases. They found that the short-term decreases presented in Svensmark et al. (2009) are not anomalous when viewed as part of a longer-term time series, and that the apparent response to Forbush decreases in Svensmark et al. (2009) was dominated by a single event on 19 January 2005. They found no evidence that the decrease in liquid water cloud fraction on 19 January 2005 or in the mean of the five events studied by

ACPD
12, 15373–15417, 2012

Svensmark et al. (2009) was causally linked to Forbush decreases. Laken et al. (2009) concluded that the observed time delay in the liquid water cloud fraction response was longer than expected if it were due to changes in the ion-induced nucleation rate.

In Laken et al. (2010), a statistical analysis of short-term decreases in cloud cover showed a correlation with decreases in GCR flux. Rather than examine cloud properties during periods of unusual activity in GCR flux, they found periods during which satellite observations of visible and infrared clouds underwent abrupt change. Laken et al. (2010) found that when mid-latitude clouds experienced a relative decrease over a short time scale, GCR flux also underwent a statistically significant decrease. They concluded that short-term changes in the cosmic ray flux are likely to affect cloud properties under suitable atmospheric conditions, but it was unlikely to be via a first-order effect such as ion-induced nucleation.

Čalogović et al. (2010) performed a statistical comparison of infrared ISCCP cloud cover data (Rossow, 1996) with changes in the atmospheric ionisation rate caused by Forbush decreases. By using $5 \times 5^{\circ}$ grid boxes with a temporal resolution of three hours, they were able to improve their statistical analysis compared with previous cosmic ray-cloud comparisons, which looked at monthly global means (e.g. Marsh and Svensmark, 2000). They tested for correlations at three different altitude levels across a range of time lags from 0 to 10 days. They concluded that the small correlation found in the cloud data was not caused by changes in the GCR flux. Laken and Čalogović (2011) also conclude that none of the solar effects examined in the paper (changes in total solar irradiance, GCR flux, and 10.7 cm solar radio flux) corresponds to a statistically significant change in cloud cover.

In the most recent study, Svensmark et al. (2012) examined MODIS data for six variables for the same five Forbush decreases used in Svensmark et al. (2009). They again concluded that they had observed a response to Forbush decreases in the MODIS data at various significance levels but independent analyses reached the opposite conclusion (Rypdal, 2012; Laken and Čalogović, 2012; Dunne, 2012).

ACPD
12, 15373–15417, 2012

Bondo et al. (2010) used a box model to test the response of marine aerosol optical properties to a change in the ionisation rate. They modelled secondary aerosol formation in the presence of a population of primary sea-salt aerosol, and its subsequent growth via condensation of sulphuric acid and coagulation. They then calculated the aerosol optical depth from the modelled size distribution. The microphysical processes employed by Bondo et al. (2010) were relatively simplistic. Their nucleation rate was assumed to be constant aside from a linear dependence on ion concentrations. Nucleation is a complex process with strong dependencies on, for example, temperature and sulphuric acid concentration. Bondo et al. (2010) do not include a diurnal cycle in their sulphuric acid production rate.

Bondo et al. (2010) suggested that the decrease in Ångström exponent observed by Svensmark et al. (2009) was caused by an increase in aerosol effective radius due to a reduction in nucleation. They were able to tune the parameters used in their model to produce a decrease in the Ångström exponent. However, their simulations had unusually high production rates of sulphuric acid and low nucleation rate – conditions which would cause the greatest sensitivity to the nucleation rate, but are not consistent with atmospheric observations. The modelled sulphuric acid production rate of $P_{H_2SO_4} = 20\,000\,\mathrm{cm^{-3}\,s^{-1}}$ led to a sulphuric acid concentration of $5 \times 10^7\,\mathrm{cm^{-3}}$, which is higher than expected in a marine environment. For example, Berresheim et al. (2002) found daily mean H_2SO_4 concentrations of $2.6 \times 10^6\,\mathrm{cm^{-3}}$ in coastal air in June 1999, with a mean daily maximum of $1.04 \times 10^7\,\mathrm{cm^{-3}}$. Concentrations are likely to be much lower over remote ocean regions. At these concentrations, the activation nucleation mechanism of Kulmala et al. (2006) would predict a nucleation rate of $J_{\mathrm{act},1.5} = 2\times10^{-6}\times5\times10^7 = 100\,\mathrm{cm^{-3}\,s^{-1}}$ (assuming a rate coefficient $A = 2\times10^{-6}\,\mathrm{s^{-1}}$, Sihto et al., 2006), much higher than the constant background rate of $0.001\,\mathrm{cm^{-3}\,s^{-1}}$ assumed by Bondo et al. (2010). Thus Bondo et al. (2010)'s idealised simulations appear to be outside the atmospheric range.

Snow-Kropla et al. (2011) used a global aerosol microphysics model to test the response of the number concentration of particles with diameter greater than 10 nm

ACPD
12, 15373–15417, 2012

(CN_{10}) and 80 nm (CCN_{80}) and Ångström exponent to a simulated Forbush decrease. They used the ion-mediated nucleation look-up tables of Yu (2010), and calculated the ionisation rate using the method of Usoskin and Kovaltsov (2006). Snow-Kropla et al. (2011) simulated eight Forbush decrease events by changing the sun's modulation of cosmic rays from a value equivalent to solar maximum to a value equivalent to solar minimum, followed by five days of linear recovery to the solar maximum value. The simulated nucleation rate at solar minimum was 1 to 5 % higher than during solar maximum. Their methods were more sophisticated than Bondo et al. (2010), as their model accounts for several factors neglected by Bondo et al. (2010) which could dampen the sensitivity of the aerosol system to a change in nucleation, including the coagulation of secondary aerosol with primary particles, and an explicit simulation of free tropospheric nucleation. They found that the concentration of particles larger than 10 nm changed by 0.16 % and CCN with diameter greater than 80 nm changed by 0.13 % in the days following the Forbush decrease, with a delay of a week before the minimum in CCN_{80}. The delay is consistent with growth rates observed by Kulmala et al. (2004). However, they concluded that these changes would not be sufficiently large to alter cloud properties. The response in Ångström exponent was 100 times smaller than that observed in Svensmark et al. (2009). While Snow-Kropla et al. (2011) did test for significance, their figures only show a confidence interval about the percentage response, and not the significance level of the absolute change.

2 Method

We want to test the hypothesis that changes in the nucleation rate can account for observed correlations between GCRs and cloud and aerosol properties. We also aim to evaluate the response in aerosol in a way that is transferable to atmospheric observations, taking into account the detectability of the response above global aerosol variability. We do this by quantifying the response of several aerosol parameters to a change in the nucleation rate, using the global aerosol microphysics model GLOMAP.

ACPD
12, 15373–15417, 2012

2.1 Description of the aerosol model

The global aerosol microphysics model GLOMAP is an extension of the TOMCAT 3-D global chemical transport model (Chipperfield, 2006) driven by European Centre for Medium-Range Weather Forecasts (ECMWF) re-analyses. GLOMAP uses a $2.8 \times 2.8^{\circ}$ horizontal grid and has 31 vertical pressure levels. This study uses GLOMAP-bin, a two-moment sectional model that simulates both particle number concentrations and component masses of sulphate, particulate organic matter (from primary and secondary sources), sea salt, and black carbon (Spracklen et al., 2005; Merikanto et al., 2009). GLOMAP simulates nucleation, condensation of sulphuric acid and organic vapours onto pre-existing aerosol, coagulation, dry deposition and nucleation scavenging. GLOMAP has been evaluated against a wide range of global aerosol microphysical observations, including surface and free tropospheric measurements of particle concentrations (Spracklen et al., 2007, 2010; Reddington et al., 2011) and nucleation events (Spracklen et al., 2006). The model uses the AEROCOM emissions inventory for SO_2, black carbon and organic carbon. Primary carbonaceous particles are emitted assuming the log-normal size distribution suggested by (Dentener et al., 2006) (fossil fuel emissions: $D = 30$ nm, $\sigma = 1.8$; wildfire and biofuel emissions: $D = 80$ nm, $\sigma = 1.8$). Primary (sub-grid) SO_4 particles are emitted as 2.5 % of SO_2 emissions, also assuming the log-normal size distribution recommended by (Dentener et al., 2006) (road transport: $D = 30$ nm, $\sigma = 1.8$; shipping, industry and power-plant emissions: $D = 1$ µm, $\sigma = 2.0$; wildfire and biofuel emissions: $D = 80$ nm, $\sigma = 1.8$; volcanic emissions: 50 % at $D = 30$ nm and 50 % at $D = 80$ nm, $\sigma = 1.8$). The DMS emissions are driven by the sea-air transfer velocity parameterisation of Nightingale et al. (2000). Sea salt was emitted using the flux parameterisation of Smith and Harrison (1998) and Gong (2003).

Good agreement has been shown between GLOMAP and aerosol observations when using a combination of the binary homogeneous nucleation mechanism of Vehkamäki et al. (2002) in the free troposphere with a boundary layer nucleation mechanism, as described in Spracklen et al. (2006). We use the activation-based empirical

ACPD
12, 15373–15417, 2012

boundary layer nucleation mechanism of Sihto et al. (2006) to model new particle formation rates at 1.5 nm $J_{act,1.5} = 2 \times 10^{-6} s^{-1}$ [H_2SO_4]. The particles are then grown to 3 nm using the formula of Kerminen and Kulmala (2002). Typical monthly mean modelled surface nucleation rates for July are $\sim 10^{-5}$–10^{-2} cm^{-3} s^{-1} over the ocean, and 10^{-3}–10^{0} cm^{-3} s^{-1} over land. The mechanism of Sihto et al. (2006) depends only on sulphuric acid concentration and does not account for temperature or concentrations of other precursor vapours. Yu et al. (2010) and Zhang et al. (2010) show that this mechanism may significantly overpredict nucleation rates under some conditions. However, evaluation against ambient measurements shows that it is one of the best predictors of particle concentrations in the boundary layer (Spracklen et al., 2006, 2010).

Previous nucleation studies in GLOMAP have used the parametrisation of Kulmala et al. (1998), but this study uses the improved parametrisation of Vehkamäki et al. (2002). The latter is more physically accurate, as it takes the formation of sulphuric acid hydrates into account and predicts the critical cluster size. The effective change in the modelled nucleation rate is quite small, due to losses of sub-3 nm particles, so the model validation carried out with the parametrisation of Kulmala et al. (1998) remains valid (J. Merikanto, personal communication, 2012).

2.2 Design of the experiments

Our approach is to assume that the global 3-D nucleation rates in GLOMAP are approximately correct (based on agreement with observations) and to perturb these rates to test an upper limit of the effect of Forbush decreases on CCN. The scaling of the nucleation rate in the unperturbed and perturbed runs is shown in Fig. 1.

The relative proportion of nucleated particles derived from charged and neutral processes is very uncertain. Analysis of observations suggests that the contribution of ion-induced nucleation to new particle formation events is between 6 % and 15 % (Laakso et al., 2007; Boy et al., 2008; Gagné et al., 2008; Manninen et al., 2009), while one model suggests that as much as 80 % of nucleation events could be ion-mediated (Yu and Turco, 2008, 2011). We assume that all nucleation is reduced by 15 % for 10 days.

ACPD
12, 15373–15417, 2012

Depending on the relative proportions of neutral and ion-induced nucleation, the actual decrease in the nucleation rate resulting from a Forbush decrease could be much smaller than we simulate here.

The model was spun up for three months and then run for one year in control and perturbed simulations. The control simulation used the binary homogeneous nucleation parametrisation of Vehkamäki et al. (2002) in the free troposphere and an activation-based boundary layer mechanism (Sihto et al., 2006; Spracklen et al., 2006). In the perturbed simulation, the calculated nucleation rate was scaled by 0.85 throughout the atmosphere for 10 days in the middle of each 30-day period. This decrease corresponds to the largest magnitude of the Forbush decreases used by Svensmark et al. (2009) and Bondo et al. (2010). The first 10 days of each month are identical in the unperturbed and perturbed simulations. Since we do not know a priori the magnitude or timescale of the aerosol response, we analyse the full thirty-day periods rather than the ten days of reduced nucleation.

The 12 sets of 30-day periods were analysed using equal epoch analysis techniques (Forbush et al., 1983). This technique has been used in the past to amplify the signal to noise ratio when analysing responses in atmospheric ion concentrations to Forbush decreases. We assume that any response to the perturbation will occur approximately at the same time in each 30-day period. By simulating twelve different months over a full year, rather than the same month from different years, we can determine whether there is a stronger response to a short-term change in the nucleation rate at any point during the seasonal cycle. By comparing otherwise identical sets of unperturbed and perturbed simulations, we can attribute any observed change directly to the simulated short-term decrease in the nucleation rate.

We analyse three model diagnostics: the global mean concentration of aerosol particles with dry diameters greater than 10 nm (CN_{10}) and 70 nm (CCN_{70}) and the Ångström exponent $AE_{340-440}$. Aerosol optical depth (AOD) is a measure of the extinction of light of a given wavelength by aerosol scattering and absorption. When AOD has been measured for two wavelengths λ_1 and λ_2, the Ångström exponent (AE) can

ACPD
12, 15373–15417, 2012

be calculated as follows:

$$\mathrm{AE} = \frac{\log\frac{\lambda_1}{\lambda_2}}{\log\frac{\mathrm{AOD}_{\lambda_1}}{\mathrm{AOD}_{\lambda_2}}}. \quad (1)$$

The Ångström exponent provides indirect information on the aerosol size distribution; for example, in a bimodal distribution $\mathrm{AE}_{340-440}$ responds to the fine mode aerosol radius, while the Ångström exponent calculated from longer wavelength pairs would provide information on the fine mode fraction of aerosols (Schuster et al., 2006).

2.3 Statistical analysis

The purpose of the statistical tests is to determine whether some additional forcing (here a change in the nucleation rate) has increased the variability of the data beyond what would be expected from the natural fluctuations of the system. When testing for statistical significance, we first need to define a null hypothesis H_0 and then perform a test to accept or reject that null hypothesis. H_0 here is that several samples are from the same underlying population. The samples in this case are the 30 days of the 12 periods defined by the equal epoch analysis. The test of this hypothesis will be the analysis of variance (ANOVA). The aim is to identify any day in which the perturbed nucleation rate has altered the properties of the day away from the underlying population by comparing the variance within each sample to the variance across all samples. In order to remove the effect of external factors such as meteorology, we first remove the trend in each month – this is common practice in tests regarding the variance of the errors where the trend is not of interest. We also check the validity of the statistical tests before performing them.

The statistical tests used here rely on the assumptions that the errors (deviations from the mean) are independent and follow a normal distribution with homogeneous variances. The tests are robust to slight deviations from these assumptions, but may

ACPD
12, 15373–15417, 2012

be invalid with large deviation (Forbush et al., 1982), so we test the errors for both normality and homogeneity of variances. The data are known to contain autocorrelations and therefore the assumption of independence is violated. If necessary, the tests can be corrected in the presence of autocorrelations as discussed in Sect. 2.3.5.

2.3.1 Removal of trend

Over the course of a year, concentrations of atmospheric aerosol change substantially. These changes make it difficult to extract the signal of interest. We process our data to remove linear trends from each month without changing the properties of the deviations from this trend that are the focus of our analysis. None of the papers cited in Sect. 1 investigating the Forbush decrease-cloud link removed trends from the data, meaning that the spread between epochs would smear an underlying normal distribution.

The 360 data points (Y_{ij}) are divided into $I = 12$ samples of $J = 30$ observations. We fit a line to each of the $i = 1,..., 12$ months' data, with slope m_i and intercept c_i, where the abscissa values j are the days of the month:

$$Y_{ij} = m_i j + c_i. \quad (2)$$

A new data set is defined as

$$X_{ij} = Y_{ij} - m_i j - c_i. \quad (3)$$

2.3.2 Testing for normality

If the true distribution is different from a normal distribution, the results of these tests may not be valid. For example, if the distribution has fat tails, fluctuations that are within the true 95 % confidence interval can be found to be statistically significant using tests designed for normal distributions. It is widely assumed that data are normal, although it is less common to use statistical tests to confirm normality. It is important to choose an appropriate test for the data; if there are strong autocorrelations the null hypothesis of normality can be incorrectly rejected.

ACPD
12, 15373–15417, 2012

To determine whether our Ångström exponent and concentrations of CN_{10} and CCN_{70} are normally distributed, the Lilliefors test was applied (Lilliefors, 1967). The Lilliefors test is a modified Kolmogorov-Smirnov test (Massey, 1951), which does not require that the normal distribution to which the sample belongs be specified. The Kolmogorov-Smirnov test is a more robust test of normality than the Shapiro-Wilk test when dealing with the autocorrelations present in time series (Shapiro and Wilk, 1965; Durilleul and Legendre, 1992). The null hypothesis used in this test is that the data are normally distributed.

2.3.3 Testing for homogeneous variances

Forbush et al. (1983) highlight the problems associated with carrying out an analysis of atmospheric data. They give a detailed step-by-step process for carrying out an equal epoch analysis correctly. One step is the testing of variances between days to confirm their homogeneity - that is, that each day has approximately the same variance between months. We use the Brown-Forsythe test for homogeneity of variances (Brown and Forsythe, 1974). We define a new data set $Z_{ij} = |X_{ij} - \bar{X}_{.j}|$ and compare the test statistic W against F_α for $(J-1, IJ-J)$ degrees of freedom, where

$$W = \left[(IJ-J) \sum_{j=1}^{J=30} I(Z_{.j} - Z_{..})^2 \right] / \left[(J-1) \sum_{j=1}^{J=30} \sum_{i=1}^{I=12} (Z_{ij} - Z_{.j})^2 \right]. \quad (4)$$

2.3.4 Plotting the data

A useful step in any statistical analysis is to visualise the data. When the normality assumption has been verified we can draw meaningful confidence intervals around the data for each day and plot it. This will help us to understand the results of any statistical tests and their conclusions. To give a sense of scale, we have added the ensemble mean of the unprocessed data $\bar{Y} = \sum_{i=1}^{I} \sum_{j=1}^{J} Y_{ij}/IJ$ back to each data point X_{ij} when plotting graphs. This has no effect on the statistical analysis.

ACPD
12, 15373–15417, 2012

For a normally distributed population, with mean μ and standard deviation σ, 95 % of the distribution lies within two standard deviations of the mean, in the range $[\mu - 2\,\sigma, \mu + 2\,\sigma]$. When we have only a sample from the population, however, we should instead use Student's t-statistic to calculate the 95 % confidence interval from the sample mean $\bar{X}$ and the sample standard deviation S. The interval $[\bar{X} - t_{\alpha/2,N-1}S, \bar{X} + t_{\alpha/2,N-1}S]$ is estimated to contain $(1-\alpha)$ of the population from which the sample has been drawn, where α is the confidence level (usually 0.05), N is the sample size, and $t_{\alpha/2,N-1}$ is Student's t-statistic for confidence level α and $(N-1)$ degrees of freedom.

We form a time series of 30 daily means $\bar{X}_{\cdot j}$ for each day of the 12 combined months, and for each of these means we have a sample variance calculated for that day from the $I = 12$ months:

$$S_j = \sqrt{\frac{\sum_{i=1}^{I=12} (X_{ij} - \bar{X}_{\cdot j})^2}{I-1}}. \quad (5)$$

The 95 % confidence interval of each day's distribution is then

$$\bar{X}_{\cdot j} \pm t_{\alpha/2,I-1} S_j. \quad (6)$$

The 95 % confidence interval for the true mean μ of a population from a sample is

$$\mu = \bar{X} \pm t_{\alpha/2,N-1} S/\sqrt{N}. \quad (7)$$

The size of the confidence interval about the mean is reduced by increasing the sample size.

2.3.5 Dealing with autocorrelation in the data

Atmospheric data generally contain autocorrelations, resulting in their not being sequentially independent. Forbush et al. (1982) do not discuss autocorrelation, but instead focus on the similar phenomenon of quasi-persistency. Quasi-persistency occurs

ACPD
12, 15373–15417, 2012

when a data set includes a periodic signal, and sequential epochs of approximately the length of the period are analysed. The periodicity will lead to correlation between epochs. Both autocorrelated and quasi-persistent data have a smaller variance about their mean than would be the case for independent data.

When dealing with autocorrelated data, the number of independent data points (effective sample size) is calculated and used to scale the sample variance (Wilks, 1997). This results in a larger confidence interval than when autocorrelations are neglected, making it less likely that a response will be deemed statistically significant. For data with quasi-persistency, the number of independent epochs (effective length of sequences) is equivalent, and should be accounted for when testing for significance (Forbush et al., 1983). Because aerosol properties are not periodic on monthly timescales, we do not need to account for quasi-persistency in our data.

2.3.6 Analysis of variance (ANOVA)

To determine whether any of the days is statistically significantly different from the others we use analysis of variance (ANOVA), otherwise known as the F-test. If our modelled change in the nucleation rate causes a statistically significant response on any day of the month, the F-test will detect it. Our experimental design is equivalent to a randomised block design examining $I \times J$ observations divided into I blocks of J observations.

The signal variance between days is

$$S_c^2 = I \sum_{j=1}^{J=30} (\bar{X}_{.j} - \bar{X}_{..})^2/(J-1). \quad (8)$$

The signal variance between months or epochs is

$$S_r^2 = J \sum_{i=1}^{I} (X_{i.} - \bar{X}_{..})^2/(I-1). \quad (9)$$

ACPD
12, 15373–15417, 2012

We expect S_r^2 to be small due to the processing described in Sect. 2.3.1. The total variance is

$$S_T^2 = \sum_{i=1}^{I} \sum_{j=1}^{J} (X_{ij} - \bar{X}_{..})^2 / (IJ - 1) \tag{10}$$

and the residual variance is

$$S_R^2 = \frac{(IJ-1)S_T^2 - (J-1)S_c^2 - (I-1)S_r^2}{(I-1)(J-1)}. \tag{11}$$

The method of Forbush et al. (1983) uses an estimate of the variance between measurements on different days (S_c^2), and an estimate of the residual variance of all measurements (S_R^2). The ratio of these estimates, F, is then compared with a critical value F_α, which depends on the degrees of freedom of the two estimates of variance. If $F = S_c^2/S_R^2 > F_\alpha$, the null hypothesis that the variance between days is smaller than the residual variance is rejected.

We are considering 30 samples of 12 measurements. This means that the numerator has $J-1 = 29$ degrees of freedom, and the denominator has $(J-1)(I-1) = 319$ degrees of freedom. This gives a value of $F_\alpha = 1.5032$ for a confidence level of $\alpha = 0.05$. If we were attempting to show that $S_c^2 = S_R^2$, then if $F < 1$ we would test $1/F$ against $F_\alpha(\alpha/2, (J-1)(I-1), (J-1))$ (Hald, 1952). However, we are satisfied with demonstrating that the variance between days S_c^2 is less than or equal to the residual variance of the system S_R^2.

Because the days were not assigned randomly to blocks, but are part of a defined sequence, autocorrelations between days would be expected to increase the value of S_c^2. However, when we took autocorrelations into account, we found that the value of S_R^2 also increased, and as a result F was found to decrease. The changes in degrees of freedom would also have resulted in an increase in F_α. Our conclusions would have remained unchanged, so we chose to neglect autocorrelations during our analysis.

ACPD
12, 15373–15417, 2012

We will carry out the same analysis on each of the outputs listed in Sect. 2.1 for both the perturbed and unperturbed data. The outputs will be tested as a global mean and also at the grid box level so that regional effects of the Forbush decrease can be identified. Furthermore, the perturbed and unperturbed data sets will be compared to identify any effect of the change in the nucleation rate even when this is shown not to be significant.

3 Results and discussions

Changes in aerosol concentrations were examined at three different altitude levels: the surface model level, 1–3 km and 10–15 km a.s.l. The surface model layer is of interest because it is where most real-world observations are made. Altitudes of 1–3 km include low clouds that are sensitive to changes in CCN. Both the highest ionisation rates due to cosmic rays and the largest response to a change in incoming GCR flux occur at altitudes of about 10–15 km. Nucleation is also the dominant source of aerosol at this altitude, so one would expect that any response in aerosol properties would be particularly noticeable. Ångström exponent is a column-integrated quantity.

We describe the analysis of surface CCN_{70} in detail, followed by a summary of the findings for the other quantities.

3.1 Global mean surface CCN_{70}

3.1.1 Testing for normality

Surface CCN_{70} were subjected to the Lilliefors test after de-trending (Sect. 2.3.1). The de-trended surface CCN_{70} for each month are shown as a time series in Fig. 2. Removing the trend in each month allows us to analyse all 360 data points as a single sample. The probability distributions for de-trended and raw surface CCN_{70} in Fig. 3 show that the raw data has a much wider spread with two small peaks. The difference between

ACPD
12, 15373–15417, 2012

the raw and de-trended distributions shows the importance of correctly processing the data before carrying out statistical tests.

The results of the Lilliefors and Brown-Forsythe tests on de-trended data are shown in Table 1. P is the probability of obtaining a test statistic of equal or greater value than observed, in the case where the null hypothesis is true. A larger p-value means that data are more likely to be normally distributed. If the test statistic KSTAT is larger than the tabulated critical value for a given sample size, the null hypothesis that the data are normally distributed is rejected. Table 1 shows that the null hypothesis of normality was not rejected for surface CCN_{70}. The Brown-Forsythe test found that the variances on different days of the month were slightly inhomogeneous, but according to Forbush et al. (1982), moderate departures from homogeneous variances will not have a large effect on the results of the tests.

3.1.2 Testing for significance

The F-test was used to determine whether the aerosol properties exhibited a statistically significant difference on any day of the month. We initially tested the model control (unperturbed) run, to confirm that any observed significance in the perturbed data was due solely to the decrease in the nucleation rate. The results of the F-tests on unperturbed and perturbed data are shown in Table 2.

We calculated the variance between different days S_c^2 (Eq. 8) and the residual variance of the data S_R^2 (Eq. 11).

$S_c^2 = 84.4401$

$S_R^2 = 141.724.$

Their ratio is $F = 0.596 < F_\alpha = 1.5032$. Thus the null hypothesis that all days are drawn from the same overall population was not rejected. The same calculations were then carried out using the perturbed data.

ACPD
12, 15373–15417, 2012

$S_c^2 = 85.7378$

$S_R^2 = 142.263$

$$F = \frac{85.7378}{142.263} = 0.603 < F_\alpha = 1.5032$$

The null hypothesis that all days are drawn from the same overall population was not rejected.

Figure 4a shows the time series of daily mean surface CCN_{70}, with the error bars showing the 95 % confidence interval of the daily distributions (Eq. 6). The solid horizontal line shows the ensemble mean, and the dashed horizontal lines give the 95 % confidence interval in estimating the mean (Eq. 7). Figure 4b shows the individual data points, rather than daily means and confidence intervals. The solid horizontal line shows again the ensemble mean, but the dashed lines now give the 95 % confidence interval of the ensemble distribution $[\bar{X} - t_{\alpha/2,N-1}S, \bar{X} + t_{\alpha/2,N-1}S]$. We would expect 95 % of the data points to lie within this confidence interval, meaning that 18 points can fall outside of it. Perturbed data points are no more likely to fall outside the confidence interval than unperturbed. If autocorrelations in the data were taken into account, the confidence interval would be larger, and fewer points would fall outside of it.

Our analysis shows that a 15 % change in nucleation rate throughout the atmosphere does not lead to a response in surface CCN_{70} that is statistically significant within the noise of natural variability. The maximum absolute difference between perturbed and unperturbed surface CCN_{70} is 0.7 cm^{-3}, which occurs 12 days after the onset of the perturbation, on day 22 of the epoch (Table 4). The response is equivalent to only a 0.15 % change in CCN concentration and is comparable in magnitude to the percentage change calculated by Snow-Kropla et al. (2011).

ACPD
12, 15373–15417, 2012

3.2 Results for other parameters

3.2.1 Global mean statistics

The results of the Lilliefors test and the Brown-Forsythe test for all global mean data are given in Table 1, and the results of the F-test in Table 2. No statistically significant response in aerosol concentrations or optical properties was calculated.

Global mean CN_{10} concentrations respond much more quickly and more strongly to changes in the nucleation rate than CCN_{70}, because the response of CCN_{70} is damped by the coagulation losses of nuclei as they grow to 70 nm. Responses of CN and CCN are compared in Figs. 4 and 5; only CN_{10} concentrations decrease noticeably during the period of reduced nucleation, by about 10.9 cm^{-3} against a mean value of about 1064 cm^{-1}. The response in CN_{10} is strongest at the surface because the nucleation rate in the boundary layer $J_{BLN} = A\,[H_2SO_4]$ is higher than in the free troposphere, so the 15 % decrease in the nucleation rate has a larger effect. A nucleation mechanism depending on the ionisation rate would tend to have a maximum effect in the free troposphere. However, even with an upper limit assumption of nucleation in the boundary layer the response is not statistically significant.

At 10–15 km the model predicts that the concentrations of CN_{10} and CCN_{70} increase slightly in response to a decrease in nucleation rate. This may be caused by the decreased competition for condensable vapour during the period of reduced nucleation, allowing existing particles to grow up to CCN sizes. It should be noted that the null hypothesis of normality was rejected for CCN_{70} at 10–15 km. Since Forbush et al. (1983) recommend caution in accepting the significance of a signal rather than rejecting it, we suggest that our conclusions about significance are valid despite the lack of normality in CCN_{70}. Figure 6 shows the raw and detrended CCN_{70} distributions at 10–15 km altitude. The rejection of the null hypothesis of normality is most likely due to the distribution's fat tails.

ACPD
12, 15373–15417, 2012

The null hypothesis of normality was also rejected for Ångström exponent. Figure 7 suggests that in the case of the Ångström exponent, the population's distribution is thin-tailed; no data points fall outside of the calculated 95 % confidence interval of the ensemble mean. The thin-tailed $AE_{340-440}$ distribution implies that the true expected variability is smaller than would be accounted for by an F-test.

3.2.2 Model grid point statistics

To take advantage of the full spatial resolution of our global aerosol microphysics model, we have performed the F-test on CN_{10} and CCN_{70} in each of the 253,952 grid boxes, and $AE_{340-440}$ for each integrated column. Table 3 shows the proportion of unperturbed and perturbed grid boxes for which the variation between days is found to be statistically significantly greater than the residual variance in that grid box.

Perturbing the nucleation rate causes a small increase in the number of grid boxes for which the null hypothesis is rejected (that is, for which $F = S_c^2/S_R^2 > F_\alpha$) for both CN_{10} and CCN_{70}, but a small decrease in the case of $AE_{340-440}$. No distinctive pattern in the response over land or ocean was observed. Figure 4 shows the number of model altitude levels for which $F > F_\alpha$ in the case of unperturbed CN_{10}. Large local variations in CN_{10} concentrations will result in higher F-values. Figure 4 shows the difference in regional significance between unperturbed and perturbed data sets. The differences are small and do not show any kind of geographical trend. At the surface there is a mean increase in grid boxes where $F > F_\alpha$ of ~1 % for CN_{10} but only a 0.15 % increase for CCN_{70}.

Table 4 shows the maximum difference between perturbed and unperturbed data averaged over 12 months. The largest difference at 1–3 km is 1.18 % for CN_{10} and 0.18 % for CCN_{70}. Table 5 shows the maximum difference between perturbed and unperturbed data from each day in the year.

ACPD
12, 15373–15417, 2012

4 Conclusions

The two main questions concerning possible correlations between cosmic ray fluctuations and aerosol and cloud properties (Svensmark et al., 2009) are whether the observed correlations are causally linked and, if so, what mechanism could link them on the time scale of days. Laken et al. (2009), Čalogović et al. (2010) and Laken and Čalogović (2011) all concluded that the observed correlations were not causally linked to Forbush decreases. Laken et al. (2010) suggested that under the right conditions, a change in the GCR flux might affect cloud cover, but that it was unlikely to be via the mechanism of ion-induced nucleation. To date, none of the papers looking at the response of cloud and aerosol properties to Forbush decreases has used superposed epoch analysis, and this is likely to affect the validity of their findings.

Here we have tested the significance of changes in CN and CCN in response to transient reductions in the nucleation rate in a global aerosol model. Although we have limited our study to perturbations of the neutral nucleation rate, the applied decrease in the nucleation rate is comparable to or slightly larger than the decrease that would occur after the strongest Forbush decreases assuming all nucleation is ion-induced. The estimated fraction of nucleated particles derived from ion-mediated processes varies between 6 to 15 % based on observations (Boy et al., 2008; Gagné et al., 2008; Manninen et al., 2009) to about 80 % in the model of Yu and Turco (2008, 2011).

Under well-controlled model conditions and with a known control aerosol state, our model produces a response in global mean surface CN_{10} of 1.03 % and in CCN_{70} of 0.15 % based on the superposition of 12 Forbush-type events through the year. Our value for CCN_{70} compares well with Snow-Kropla et al. (2011)'s figure of 0.13 % for CCN_{80}. Our value for CN_{10} is larger than their figure of 0.16 %, which is to be expected for two reasons: the change in ion concentrations near the surface is smaller than in the free troposphere, leading to a response in their ion-mediated nucleation parametrisation smaller than 15 %; and our boundary layer nucleation mechanism will generate much larger nucleation rates, leading to a larger absolute change in the nucleation

ACPD
12, 15373–15417, 2012

rate. However, several statistical tests in our study show that these changes in CN_{10} and CCN_{70} would not be sufficiently greater than natural variability to be detectable in a blind study in which the control aerosol state is not known.

Our study agrees with that of Snow-Kropla et al. (2011) that the model-predicted changes in CN and CCN would not be sufficiently large to generate Svensmark et al. (2009)'s observed changes in cloud properties. Thus, based on two fairly sophisticated global models and independent assumptions about the nucleation processes, transient decreases in nucleation rate accompanying Forbush events would not result in a global mean response in aerosol or cloud properties that is detectable above natural variability.

We have also questioned the very existence of a correlation between aerosol and cloud properties and Forbush events (Dunne, 2012). The statistical analyses we have applied here go beyond those used in Svensmark et al. (2012) to detect significant changes in aerosol properties. While Svensmark et al. (2012) looked for aerosol changes that were outside the 95 % confidence interval, they did not remove the trend from each epoch being analysed, nor did they test for normality of the underlying data. We have argued (Dunne, 2012) that the approach of Svensmark et al. (2012), which is much less rigorous than for example that of Forbush et al. (1983), could lead to false positives. Thus, we suggest that our model results are consistent with the observations analysed in Svensmark et al. (2012), which we argue do not reveal a statistically significant response of global aerosol to Forbush events.

The principal limitation of our study is that we have used a large-scale global model that can only resolve processes operating on the scale of greater than about 100 km. While the model nucleation processes on this scale result in spatial and temporal patterns in CN that agree fairly well with observations (Spracklen et al., 2006, 2008, 2010; Reddington et al., 2011), we cannot preclude the existence of ion-aerosol processes operating on smaller scales. For example, nucleation in the near-cloud environment under highly perturbed conditions of aerosol, trace vapours and ion density may behave differently to the kind of events that the global model has been set up to capture:

ACPD
12, 15373–15417, 2012

namely, nucleation events that are known to occur on large spatial scales (Hussein et al., 2008, 2009). We have also not addressed the possibility of cloud responses to changes in electrification, as studied by Tinsley et al. (2000); Tripathi and Harrison (2002); Harrison and Ambaum (2008, among others).

Acknowledgements. The authors would like to thank Jeff Pierce for very helpful discussion. This research has received funding from the EC's Seventh Framework Programme under grant agreement no. 215072 (Marie Curie Initial Training Network "CLOUD-ITN"). F_α was calculated using the single-calculation tool from http://www.stattools.net/FTest_Pgm.php.

References

Beard, K. V., Ochs, H. T., and Twohy, C. H.: Aircraft measurements of high average charges on cloud drops in layer clouds, Geophys. Res. Lett., 31, 4 pp., 2004. 15375

Berresheim, H., Elste, T., Tremmel, H. G., Allen, A. G., Hansson, H., Rosman, K., Dal Maso, M., Mäkelä, J. M., Kulmala, M., and O'Dowd, C. D.: Gas-aerosol relationships of H_2SO_4, MSA, and OH: observations in the coastal marine boundary layer at Mace Head, Ireland, J. Geophys. Res., 107, 12 pp., 2002. 15379

Bond, G., Kromer, B., Beer, J., Muscheler, R., Evans, M. N., Showers, W., Hoffmann, S., Lotti-Bond, R., Hajdas, I., and Bonani, G.: Persistent solar influence on north Atlantic climate during the holocene, Science, 294, 2130–2136, 2001. 15374

Bondo, T., Enghoff, M. B., and Svensmark, H.: Model of optical response of marine aerosols to Forbush decreases, Atmos. Chem. Phys., 10, 2765–2776, doi:10.5194/acp-10-2765-2010, 2010. 15378, 15379, 15380, 15383

Boy, M., Kazil, J., Lovejoy, E., Guenther, A., and Kulmala, M.: Relevance of ion-induced nucleation of sulfuric acid and water in the lower troposphere over the boreal forest at northern latitudes, Atmos. Res., 90, 151–158, 2008. 15382, 15395

Brown, M. B. and Forsythe, A. B.: Robust tests for the equality of variances, J. Am. Stat. Assoc., 69, 364–367, 1974. 15386

Čalogović, J., Albert, C., Arnold, F., Beer, J., Desorgher, L., and Flueckiger, E. O.: Sudden cosmic ray decreases: No change of global cloud cover, Geophys. Res. Lett., 37, L03802, doi:10.1029/2009GL041327, 2010. 15378, 15395

ACPD

12, 15373–15417, 2012

Carslaw, K. S., Harrison, R. G., and Kirkby, J.: Cosmic rays, clouds, and climate, Science, 298, 1732–1737, 2002. 15375
Chipperfield, M. P.: New version of the TOMCAT/SLIMCAT off-line chemical transport model: Intercomparison of stratospheric tracer experiments, Q. J. Roy. Meteor. Soc., 132, 1179–1203, 2006. 15381
Dentener, F., Kinne, S., Bond, T., Boucher, O., Cofala, J., Generoso, S., Ginoux, P., Gong, S., Hoelzemann, J. J., Ito, A., Marelli, L., Penner, J. E., Putaud, J.-P., Textor, C., Schulz, M., van der Werf, G. R., and Wilson, J.: Emissions of primary aerosol and precursor gases in the years 2000 and 1750 prescribed data-sets for AeroCom, Atmos. Chem. Phys., 6, 4321–4344, doi:10.5194/acp-6-4321-2006, 2006. 15381
Dunne, E. M.: Interactive comment on "Effects of cosmic ray decreases on cloud microphysics" by J. Svensmark et al., Atmos. Chem. Phys. Discuss., 12, C1000, 2012. 15378, 15396
Durilleul, P. and Legendre, P.: Lack of robustness in two tests of normality against autocorrelation in sample data, J. Stat. Comput. Sim., 42, 79–91, 1992. 15386
Eichler, A., Olivier, S., Henderson, K., Laube, A., Beer, J., Papina, T., Gäggeler, H. W., and Schwikowski, M.: Temperature response in the Altai region lags solar forcing, Geophys. Res. Lett., 36, L01808, doi:10.1029/2008GL035930,2009. 15374
Enghoff, M. B., Pedersen, J. O. P., Uggerhøj, U. I., Paling, S. M., and Svensmark, H.: Aerosol nucleation induced by a high energy particle beam, Geophys. Res. Lett., 38, 4 pp., 2011. 15376
Forbush, S. E.: On the effects in cosmic-ray intensity observed during the recent magnetic storm, Phys. Rev., 51, 1108–1109, 1946. 15376
Forbush, S., Duggal, S., Pomerantz, M., and Tsao, C.: Random Fluctuations, Persistence, and Quasi-Persistence in Geophysical and Cosmical Periodicities: A Sequel, Rev. Geophys. Space Ge., 20, 971–976, 1982. 15385, 15387, 15391, 15405
Forbush, S., Pomerantz, M., Duggal, S., and Tsao, C.: Statistical considerations in the analysis of solar oscillation data by the superposed epoch method, Sol. Phys., 82, 113–122, 1983. 15383, 15386, 15388, 15389, 15393, 15396
Gagné, S., Laakso, L., Petäjä, T., Kerminen, V., and Kulmala, M.: Analysis of one year of Ion-DMPS data from the SMEAR II station, finland, Tellus B, 60, 318–329, 2008. 15382, 15395
Gong, S. L.: A parameterization of sea-salt aerosol source function for sub- and super-micron particles, Global Biogeochem. Cy., 17, 7 pp., 2003. 15381
Haigh, J.: The impact of solar variability on climate, Science, 272, 981–984, 1996. 15375

ACPD
12, 15373–15417, 2012

Haigh, J. D., Winning, A. R., Toumi, R., and Harder, J. W.: An influence of solar spectral variations on radiative forcing of climate, Nature, 467, 696–699, 2010. 15375
Hald, A.: Statistical Theory with Engineering Applications, John Wiley & Sons, 1952. 15389
Harrison, R. G.: Discrimination between cosmic ray and solar irradiance effects on clouds, and evidence for geophysical modulation of cloud thickness, P. Roy. Soc. A-Math. Phy., 464, 2575–2590, 2008. 15375
Harrison, R. G. and Ambaum, M. H. P.: Enhancement of cloud formation by droplet charging, P. Roy. Soc. A-Math. Phy., 464, 2561–2573, 2008. 15375, 15397
Harrison, R. G., Ambaum, M. H. P., and Lockwood, M.: Cloud base height and cosmic rays, P. Roy. Soc. A-Math. Phy., 467, 2777–2791, 2011. 15375
Hussein, T., Martikainen, J., Junninen, H., Sogacheva, L., Wagner, R., Dal Maso, M., Riipinen, I., Aalto, P. P., and Kulmala, M.: Observation of regional new particle formation in the urban atmosphere, Tellus B, 60, 509–521, 2008. 15397
Hussein, T., Junninen, H., Tunved, P., Kristensson, A., Dal Maso, M., Riipinen, I., Aalto, P. P., Hansson, H.-C., Swietlicki, E., and Kulmala, M.: Time span and spatial scale of regional new particle formation events over Finland and Southern Sweden, Atmos. Chem. Phys., 9, 4699–4716, doi:10.5194/acp-9-4699-2009, 2009. 15397
Kazil, J., Zhang, K., Stier, P., Feichter, J., Lohmann, U., and O'Brien, K.: The present-day decadal solar cycle modulation of earth's radiative forcing via charged H_2SO_4/H_2O aerosol nucleation, Geophys. Res. Lett., 39, L02805, doi:10.1029/2011GL050058, 2012. 15376
Kerminen, V. and Kulmala, M.: Analytical formulae connecting the "real" and the "apparent" nucleation rate and the nuclei number concentration for atmospheric nucleation events, J. Aerosol Sci., 33, 609–622, 2002. 15382
Kirkby, J.: Cosmic rays and climate, Surv. Geophys., 28, 333–375, 2007. 15374
Kirkby, J., Curtius, J., Almeida, J., Dunne, E., Duplissy, J., Ehrhart, S., Franchin, A., Gagne, S., Ickes, L., Kuerten, A., Kupc, A., Metzger, A., Riccobono, F., Rondo, L., Schobesberger, S., Tsagkogeorgas, G., Wimmer, D., Amorim, A., Bianchi, F., Breitenlechner, M., David, A., Dommen, J., Downard, A., Ehn, M., Flagan, R. C., Haider, S., Hansel, A., Hauser, D., Jud, W., Junninen, H., Kreissl, F., Kvashin, A., Laaksonen, A., Lehtipalo, K., Lima, J., Lovejoy, E. R., Makhmutov, V., Mathot, S., Mikkila, J., Minginette, P., Mogo, S., Nieminen, T., Onnela, A., Pereira, P., Petaja, T., Schnitzhofer, R., Seinfeld, J. H., Sipila, M., Stozhkov, Y., Stratmann, F., Tome, A., Vanhanen, J., Viisanen, Y., Vrtala, A., Wagner, P. E., Walther, H., Weingartner, E., Wex, H., Winkler, P. M., Carslaw, K. S., Worsnop, D. R., Baltensperger, U., and Kulmala, M.:

ACPD
12, 15373–15417, 2012

Role of sulphuric acid, ammonia and galactic cosmic rays in atmospheric aerosol nucleation, Nature, 476, 429–477, 2011. 15376
Kulmala, M., Laaksonen, A., and Pirjola, L.: Parameterizations for sulfuric acid/water nucleation rates, J. Geophys. Res., 103, 8301–8307, 10.1029/97JD03718, 1998. 15382
Kulmala, M., Laakso, L., Lehtinen, K. E. J., Riipinen, I., Dal Maso, M., Anttila, T., Kerminen, V. M., Horrak, U., Vana, M., and Tammet, H.: Initial steps of aerosol growth, Atmos. Chem. Phys., 4, 2553–2560, doi:10.5194/acp-4-2553-2004, 2004. 15380
Kulmala, M., Lehtinen, K. E. J., and Laaksonen, A.: Cluster activation theory as an explanation of the linear dependence between formation rate of 3 nm particles and sulphuric acid concentration, Atmos. Chem. Phys., 6, 787–793, doi:10.5194/acp-6-787-2006, 2006. 15379
Laakso, L., Gagné, S., Petäjä, T., Hirsikko, A., Aalto, P. P., Kulmala, M., and Kerminen, V.: Detecting charging state of ultra-fine particles: instrumental development and ambient measurements, Atmos. Chem. Phys., 7, 1333–1345, doi:10.5194/acp-7-1333-2007, 2007. 15382
Laken, B. A. and Čalogović, J.: Solar irradiance, cosmic rays and cloudiness over daily timescales, Geophys. Res. Lett., 38, 6 pp., 2011. 15378, 15395
Laken, B. A. and Čalogović, J.: Interactive comment on "Effects of cosmic ray decreases on cloud microphysics" by J. Svensmark et al., Atmos. Chem. Phys. Discuss., 12, C962–C973, 2012. 15378
Laken, B., Wolfendale, A., and Kniveton, D.: Cosmic ray decreases and changes in the liquid water cloud fraction over the oceans, Geophys. Res. Lett., 36, L23803, doi:10.1029/2009GL040961, 2009. 15377, 15378, 15395
Laken, B. A., Kniveton, D. R., and Frogley, M. R.: Cosmic rays linked to rapid mid-latitude cloud changes, Atmos. Chem. Phys., 10, 10941–10948, doi:10.5194/acp-10-10941-2010, 2010. 15378, 15395
Lilliefors, H. W.: On the Kolmogorov-Smirnov test for normality with mean and variance unknown, J. Am. Stat. Assoc., 62, 399–402, 1967. 15386
Manninen, H. E., Nieminen, T., Riipinen, I., Yli-Juuti, T., Gagné, S., Asmi, E., Aalto, P. P., Petäjä, T., Kerminen, V., and Kulmala, M.: Charged and total particle formation and growth rates during EUCAARI 2007 campaign in Hyytiälä, Atmos. Chem. Phys., 9, 4077–4089, doi:10.5194/acp-9-4077-2009, 2009. 15382, 15395
Marsh, N. D. and Svensmark, H.: Low cloud properties influenced by cosmic rays, Phys. Rev. Lett., 85, 5004, doi:10.1103/PhysRevLett.85.5004, 2000. 15378

ACPD
12, 15373–15417, 2012

Massey, F. J.: The Kolmogorov-Smirnov test for goodness of fit, J. Am. Stat. Assoc., 46, 68–78, 1951. 15386
Merikanto, J., Spracklen, D. V., Mann, G. W., Pickering, S. J., and Carslaw, K. S.: Impact of nucleation on global CCN, Atmos. Chem. Phys., 9, 8601–8616, doi:10.5194/acp-9-8601-2009, 2009. 15375, 15376, 15381
Neff, U., Burns, S. J., Mangini, A., Mudelsee, M., Fleitmann, D., and Matter, A.: Strong coherence between solar variability and the monsoon in Oman between 9 and 6 kyr ago, Nature, 411, 290–293, 2001. 15374
Nightingale, P. D., Malin, G., Law, C. S., Watson, A. J., Liss, P. S., Liddicoat, M. I., Boutin, J., and Upstill-Goddard, R. C.: In situ evaluation of air-sea gas exchange parameterizations using novel conservative and volatile tracers, Global Biogeochem. Cy., 14, 373–387, 2000. 15381
Pierce, J. R. and Adams, P. J.: Efficiency of cloud condensation nuclei formation from ultrafine particles, Atmos. Chem. Phys., 7, 1367–1379, doi:10.5194/acp-7-1367-2007, 2007. 15376
Pierce, J. R. and Adams, P. J.: Can cosmic rays affect cloud condensation nuclei by altering new particle formation rates?, Geophys. Res. Lett., 36, L09820, doi:10.1029/2009GL037946, 2009a. 15376
Pierce, J. R. and Adams, P. J.: Uncertainty in global CCN concentrations from uncertain aerosol nucleation and primary emission rates, Atmos. Chem. Phys., 9, 1339–1356, doi:10.5194/acp-9-1339-2009, 2009b. 15375
Pudovkin, M. I. and Veretenenko, S. V.: Cloudiness decreases associated with Forbush-decreases of galactic cosmic rays, J. Atmos. Terr. Phys., 57, 1349–1355, 1995. 15377
Reddington, C. L., Carslaw, K. S., Spracklen, D. V., Frontoso, M. G., Collins, L., Merikanto, J., Minikin, A., Hamburger, T., Coe, H., Kulmala, M., Aalto, P., Flentje, H., Plass-Dülmer, C., Birmili, W., Wiedensohler, A., Wehner, B., Tuch, T., Sonntag, A., O'Dowd, C. D., Jennings, S. G., Dupuy, R., Baltensperger, U., Weingartner, E., Hansson, H., Tunved, P., Laj, P., Sellegri, K., Boulon, J., Putaud, J., Gruening, C., Swietlicki, E., Roldin, P., Henzing, J. S., Moerman, M., Mihalopoulos, N., Kouvarakis, G., Ždímal, V., Zíková, N., Marinoni, A., Bonasoni, P., and Duchi, R.: Primary versus secondary contributions to particle number concentrations in the european boundary layer, Atmos. Chem. Phys., 11, 12007–12036, doi:10.5194/acp-11-12007-2011, 2011. 15381, 15396
Rossow, B.: International satellite cloud climatology project (ISCCP), Technical report, Institute for Space Studies, NASA Goddard Space Flight Centre, 1996. 15378

ACPD
12, 15373–15417, 2012

Rypdal, K.: Interactive comment on "Effects of cosmic ray decreases on cloud microphysics" by J. Svensmark et al., Atmos. Chem. Phys. Discuss., 12, C247–C255, 2012. 15378
Schuster, G. L., Dubovik, O., and Holben, B. N.: Angström exponent and bimodal aerosol size distributions, J. Geophys. Res., 111, 14 pp., 2006. 15384
Shapiro, S. S. and Wilk, M. B.: An analysis of variance test for normality (Complete samples), Biometrika, 52, 591–611, 1965. 15386
Sihto, S.-L., Kulmala, M., Kerminen, V.-M., Dal Maso, M., Petäjä, T., Riipinen, I., Korhonen, H., Arnold, F., Janson, R., Boy, M., Laaksonen, A., and Lehtinen, K. E. J.: Atmospheric sulphuric acid and aerosol formation: implications from atmospheric measurements for nucleation and early growth mechanisms, Atmos. Chem. Phys., 6, 4079–4091, doi:10.5194/acp-6-4079-2006, 2006. 15379, 15382, 15383
Smith, M. and Harrison, N.: The sea spray generation function, J. Aerosol Sci., 29, 189–190, 1998. 15381
Snow-Kropla, E. J., Pierce, J. R., Westervelt, D. M., and Trivitayanurak, W.: Cosmic rays, aerosol formation and cloud-condensation nuclei: sensitivities to model uncertainties, Atmos. Chem. Phys., 11, 4001–4013, doi:10.5194/acp-11-4001-2011, 2011. 15379, 15380, 15392, 15395, 15396
Spracklen, D. V., Pringle, K. J., Carslaw, K. S., Chipperfield, M. P., and Mann, G. W.: A global off-line model of size-resolved aerosol microphysics: II. identification of key uncertainties, Atmos. Chem. Phys., 5, 3233–3250, doi:10.5194/acp-5-3233-2005, 2005. 15381
Spracklen, D. V., Carslaw, K. S., Kulmala, M., Kerminen, V., Mann, G. W., and Sihto, S.: The contribution of boundary layer nucleation events to total particle concentrations on regional and global scales, Atmos. Chem. Phys., 6, 5631–5648, doi:10.5194/acp-6-5631-2006, 2006. 15381, 15382, 15383, 15396
Spracklen, D. V., Pringle, K. J., Carslaw, K. S., Mann, G. W., Manktelow, P., and Heintzenberg, J.: Evaluation of a global aerosol microphysics model against size-resolved particle statistics in the marine atmosphere, Atmos. Chem. Phys., 7, 2073–2090, doi:10.5194/acp-7-2073-2007, 2007. 15381
Spracklen, D. V., Carslaw, K. S., Kulmala, M., Kerminen, V., Sihto, S., Riipinen, I., Merikanto, J., Mann, G. W., Chipperfield, M. P., Wiedensohler, A., Birmili, W., and Lihavainen, H.: Contribution of particle formation to global cloud condensation nuclei concentrations, Geophys. Res. Lett., 35, L06808, doi:10.1029/2007GL033038, 2008. 15396

ACPD
12, 15373–15417, 2012

Spracklen, D. V., Carslaw, K. S., Merikanto, J., Mann, G. W., Reddington, C. L., Pickering, S., Ogren, J. A., Andrews, E., Baltensperger, U., Weingartner, E., Boy, M., Kulmala, M., Laakso, L., Lihavainen, H., Kivekäs, N., Komppula, M., Mihalopoulos, N., Kouvarakis, G., Jennings, S. G., O'Dowd, C., Birmili, W., Wiedensohler, A., Weller, R., Gras, J., Laj, P., Sellegri, K., Bonn, B., Krejci, R., Laaksonen, A., Hamed, A., Minikin, A., Harrison, R. M., Talbot, R., and Sun, J.: Explaining global surface aerosol number concentrations in terms of primary emissions and particle formation, Atmos. Chem. Phys., 10, 4775–4793, doi:10.5194/acp-10-4775-2010, 2010. 15381, 15382, 15396

Svensmark, H. and Friis-Christensen, E.: Variation of cosmic ray flux and global cloud coverage – a missing link in solar-climate relationships, J. Atmos. Sol.-Terr. Phy., 59, 1225–1232, 1997. 15374, 15376

Svensmark, H., Bondo, T., and Svensmark, J.: Cosmic ray decreases affect atmospheric aerosols and clouds, Geophys. Res. Lett., 36, L15101, doi:10.1029/2009GL038429, 2009. 15377, 15378, 15379, 15380, 15383, 15395, 15396

Svensmark, J., Enghoff, M. B., and Svensmark, H.: Effects of cosmic ray decreases on cloud microphysics, Atmos. Chem. Phys. Discuss., 12, 3595–3617, doi:10.5194/acpd-12-3595-2012, 2012. 15378, 15396

Tinsley, B., Rohrbaugh, R., Hei, M., and Beard, K.: Effects of image charges on the scavenging of aerosol particles by cloud droplets and on droplet charging and possible ice nucleation processes, J. Atmos. Sci., 57, 2118–2134, 2000. 15375, 15397

Tripathi, S. N. and Harrison, R.: Enhancement of contact nucleation by scavenging of charged aerosol particles, Atmos. Res., 62, 57–70, 2002. 15375, 15397

Twomey, S.: The electrification of individual cloud droplets, Tellus, 8, 445–452, 1956. 15375

Usoskin, I. G. and Kovaltsov, G. A.: Cosmic ray induced ionization in the atmosphere: Full modeling and practical applications, J. Geophys. Res., 111, D21206, doi:10.1029/2006JD007150, 2006. 15380

Usoskin, I. G., Alanko-Huotari, K., Kovaltsov, G. A., and Mursula, K.: Heliospheric modulation of cosmic rays: Monthly reconstruction for 1951–2004, J. Geophys. Res., 110, 10 pp., 2005. 15375

Vehkamäki, H., Kulmala, M., Napari, I., Lehtinen, K. E. J., Timmreck, C., Noppel, M., and Laaksonen, A.: An improved parameterization for sulfuric acid-water nucleation rates for tropospheric and stratospheric conditions, J. Geophys. Res., 107, 4622, doi:10.1029/2006JD007150, 2002. 15381, 15382, 15383

ACPD
12, 15373–15417, 2012

Wang, P. K., Grover, S. N., and Pruppacher, H. R.: On the effect of electric charges on the scavenging of aerosol particles by clouds and small raindrops, J. Atmos. Sci., 35, 1735–1743, 1978. 15375

Wilks, D. S.: Resampling hypothesis tests for autocorrelated fields, J. Climate, 10, 65–82, 1997. 15388

Willson, R. C.: Total solar irradiance trend during solar cycles 21 and 22, Science, 277, 1963–1965, 1997. 15375

Yu, F.: Ion-mediated nucleation in the atmosphere: Key controlling parameters, implications, and look-up table, J. Geophys. Res., 115, 12 pp., 2010. 15380

Yu, F. and Luo, G.: Simulation of particle size distribution with a global aerosol model: contribution of nucleation to aerosol and CCN number concentrations, Atmos. Chem. Phys., 9, 7691–7710, doi:10.5194/acp-9-7691-2009, 2009. 15375, 15376

Yu, F. and Turco, R.: Case studies of particle formation events observed in boreal forests: implications for nucleation mechanisms, Atmos. Chem. Phys., 8, 6085–6102, doi:10.5194/acp-8-6085-2008, 2008. 15382, 15395

Yu, F. and Turco, R. P.: The size-dependent charge fraction of sub-3-nm particles as a key diagnostic of competitive nucleation mechanisms under atmospheric conditions, Atmos. Chem. Phys., 11, 9451–9463, doi:10.5194/acp-11-9451-2011, 2011. 15382, 15395

Yu, F., Luo, G., Bates, T. S., Anderson, B., Clarke, A., Kapustin, V., Yantosca, R. M., Wang, Y., and Wu, S.: Spatial distributions of particle number concentrations in the global troposphere: Simulations, observations, and implications for nucleation mechanisms, J. Geophys. Res., 115, 14 pp., doi:10.1029/2009JD013473, 2010. 15382

Zhang, K., Feichter, J., Kazil, J., Wan, H., Zhuo, W., Griffiths, A. D., Sartorius, H., Zahorowski, W., Ramonet, M., Schmidt, M., Yver, C., Neubert, R. E. M., and Brunke, E.: Radon activity in the lower troposphere and its impact on ionization rate: a global estimate using different radon emissions, Atmos. Chem. Phys., 11, 7817–7838, doi:10.5194/acp-11-7817-2011, 2011. 15375

Zhang, Y., McMurry, P. H., Yu, F., and Jacobson, M. Z.: A comparative study of nucleation parameterizations: 1. examination and evaluation of the formulations, J. Geophys. Res., 115, 23 pp., 2010. 15382

ACPD
12, 15373–15417, 2012

Table 1. Statistics returned by the Lilliefors test and the Brown-Forsythe test on Ångström exponent and on CN_{10} and CCN_{70} at the surface, 1–3 km, and 10–15 km. If the test statistic KSTAT is larger than 0.05, the null hypothesis that the data are normally distributed is rejected. The null hypothesis is rejected for CCN_{70} and $AE_{340-440nm}$. W and W' are the Brown-Forsythe test statistics for unperturbed and perturbed data respectively. If W or $W' > F_\alpha = 1.502$, the variances are not homogeneous; however, Forbush et al. (1982) say that moderate departures from homogeneous variances will not have a large effect on the results of the tests.

	H	P	KSTAT	W	W'
Surface CN_{10}	0	0.483	0.032	1.80	1.73
CN_{10} at 1–3 km	0	0.191	0.040	1.29	1.39
CN_{10} at 10–15 km	0	0.053	0.047	2.02	2.08
Surface CCN_{70}	0	>0.5	0.028	1.21	1.14
CCN_{70} at 1–3 km	0	0.153	0.041	1.51	1.42
CCN_{70} at 10–15 km	1	0.003	0.061	3.12	3.12
$AE_{340-440}$	1	0.004	0.059	1.55	1.59

ACPD
12, 15373–15417, 2012

Table 2. Results of F-tests on CN_{10}, CCN_{70} and Ångström exponent. CCN_{70} at 10–15 km and Ångström exponent are included for reference, but were found not to be normally distributed. $F_\alpha = 1.5020$.

	S_1^2	S_2^2	F	$> F_\alpha$	$S_1'^2$	$S_2'^2$	F'	$> F_\alpha$
Surface CN_{10}	395.7	423.6	0.93	No	491.2	413.19	1.19	No
CN_{10} (1–3 km)	251.4	574.8	0.44	No	503.1	560.9	0.90	No
CN_{10} (10–15 km)	466.1	2302.1	0.18	No	533.2	2298.6	0.21	No
Surface CCN_{70}	84.4	141.7	0.60	No	85.7	142.3	0.60	No
CCN_{70} (1–3 km)	55.3	106.0	0.52	No	54.1	106.4	0.51	No
CCN_{70} (10–15 km)	1.48	3.21	0.46	No	1.84	3.19	0.58	No
$AE_{340-440nm}$	0.00048	0.00060	0.80	No	0.00047	0.00060	0.78	No

ACPD
12, 15373–15417, 2012

Table 3. The number and percentage of grid boxes for which the F-test found that variance between different days of the month was statisticially significantly greater than the variance between different months. In the case of CN_{10} and CCN_{70}, there is a small increase in the number of gridboxes which have a statisticially significant F-statistic, but for $AE_{340-440}$ there is a small decrease. There are fewer grid boxes overall for $AE_{340-440}$ because it is a column-integrated quantity.

Variable	# gridboxes	# significant	% significant
Unperturbed CN_{10}	253 952	29 625	11.67 %
Perturbed CN_{10}	253 952	30 139	11.87 %
Unperturbed CCN_{70}	253 952	28 398	11.18 %
Perturbed CCN_{70}	253 952	28 529	11.23 %
Unperturbed $AE_{340-440}$	8192	1247	15.22 %
Perturbed $AE_{340-440}$	8192	1226	14.97 %

ACPD
12, 15373–15417, 2012

Table 4. The maximum absolute difference between unperturbed and perturbed data averaged over the 12 months, as both an absolute value and a percentage, as well as the day of the month on which the maximum difference occurred.

Variable	Max. abs. diff. (cm^{-3})	Max. % diff (%)	Day of month
Surface CN_{10}	10.9	1.03	20
CN_{10} at 1–3 km	9.1	1.18	19
CN_{10} at 10–15 km	5.9	0.50	13
Surface CCN_{70}	0.7	0.15	22
CCN_{70} at 1–3 km	0.7	0.18	20
CCN_{70} at 10–15 km	0.2	0.35	28
$AE_{340-440}$	0.001	0.11	22

ACPD
12, 15373–15417, 2012

Table 5. The maximum absolute difference between unperturbed and perturbed data, as both an absolute value and a percentage, as well as the day and the month on which the maximum difference occurred.

Variable	Max. abs. diff. (cm^{-3})	Max. % diff (%)	Day of month	Month
Surface CN_{10}	14.8	1.39	20	Mar
CN_{10} at 1–3 km	12.6	1.57	17	Jan
CN_{10} at 10–15 km	14.8	1.27	22	Jul
Surface CCN_{70}	1.8	0.37	18	Mar
CCN_{70} at 1–3 km	1.5	0.42	19	Jun
CCN_{70} at 10–15 km	0.8	1.23	28	Jun
$AE_{340-440}$	0.003	0.28	15	Mar

ACPD
12, 15373–15417, 2012

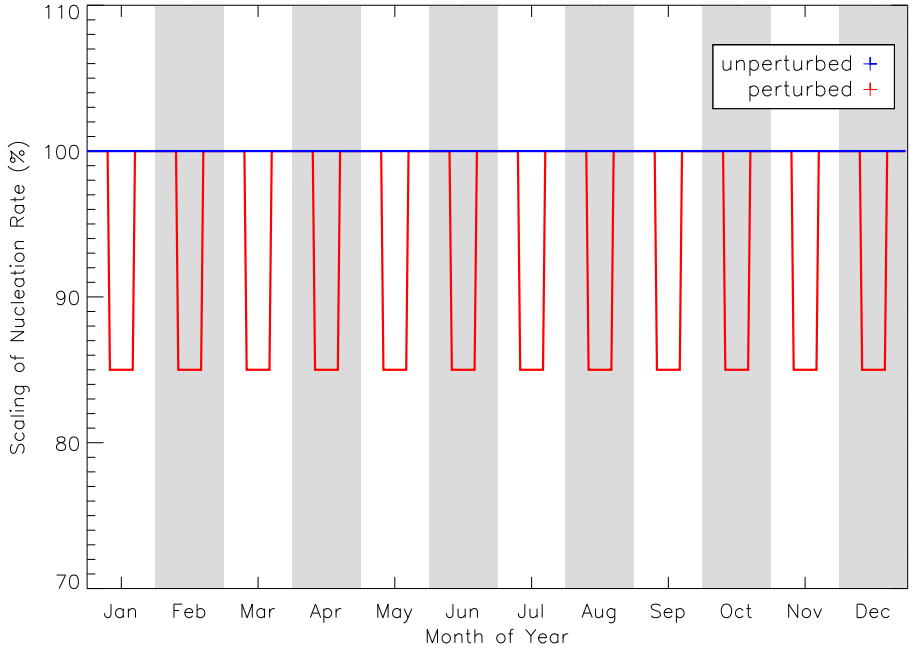

Fig. 1. Schematic of how the nucleation rate is scaled throughout the year. In the perturbed simulations (red), the nucleation rate was scaled to 85 % of its calculated value for the middle ten days of each month.

ACPD
12, 15373–15417, 2012

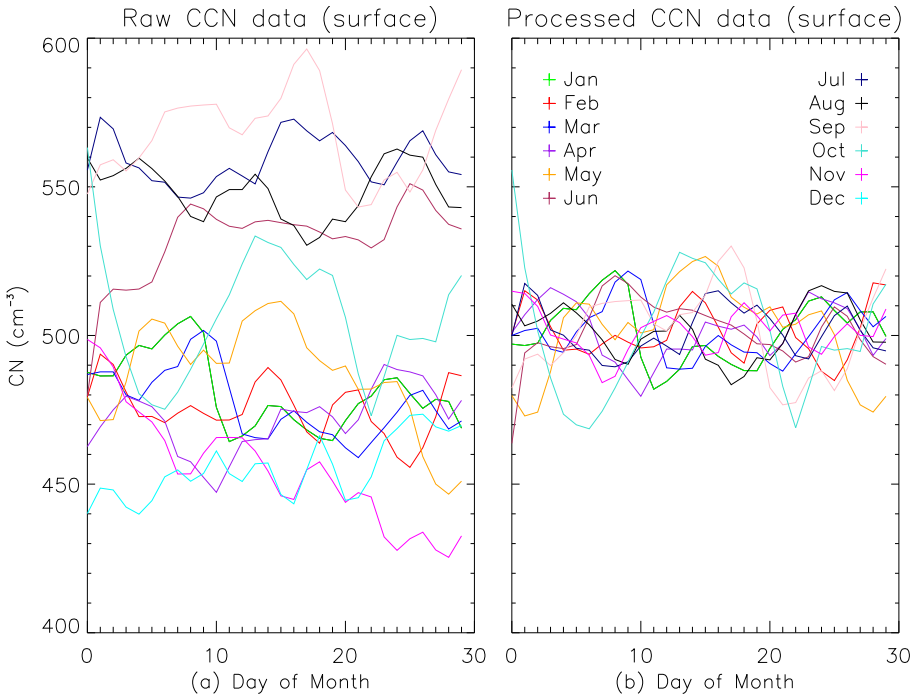

Fig. 2. Time series of unprocessed (left panel) and processed (right panel) surface CCN_{70} concentrations. The removal of the trend makes it possible to analyse the 12 samples together, but the intra-sample variance remains unchanged. The ensemble mean has been added back to each data set for graphical purposes.

ACPD
12, 15373–15417, 2012

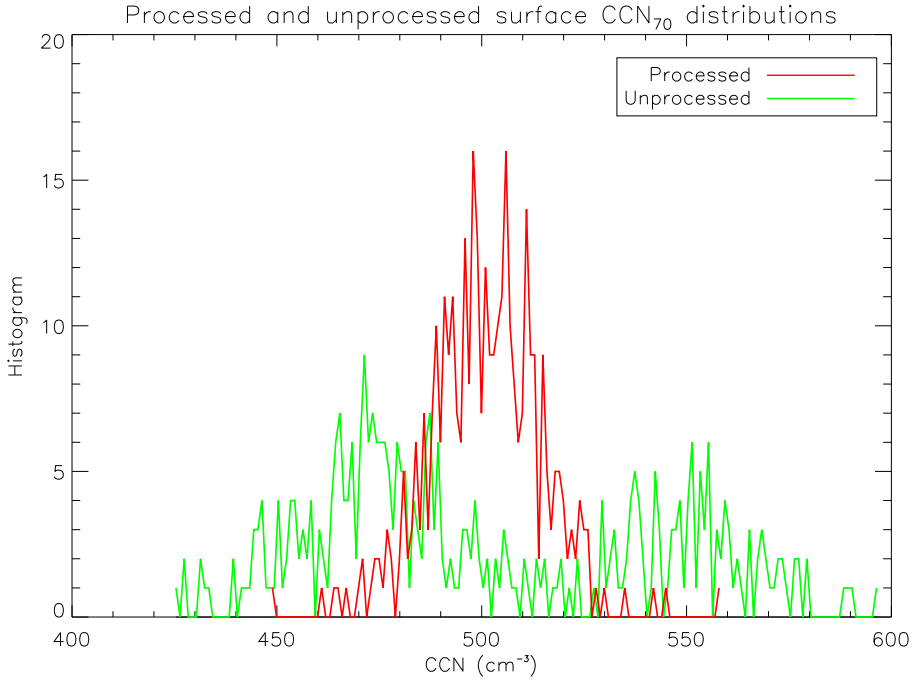

Fig. 3. Histograms showing the distribution of processed and unprocessed surface CCN_{70} concentrations. The null hypothesis that the red line (processed) is normally distributed is not rejected by the Lilliefors test.

ACPD
12, 15373–15417, 2012

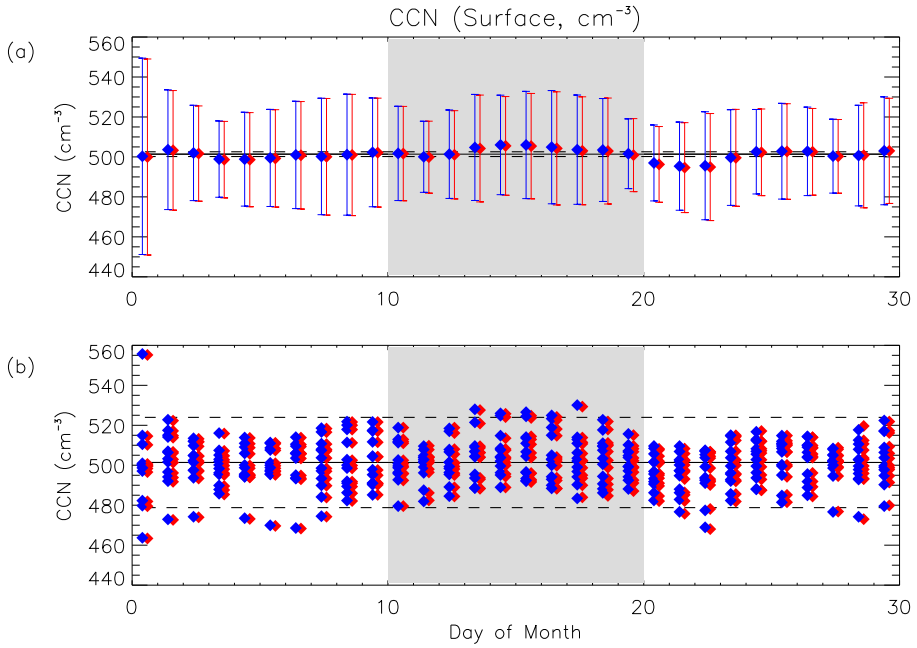

Fig. 4. Surface-level CCN. In both parts of each plot, the solid horizontal line shows the mean of all 360 measurements. Blue diamonds represent unperturbed values, and red diamonds represent perturbed values. **(a)** The dashed horizontal lines show the uncertainty on the mean, as given in Eq. (7). The diamonds show the daily means, and the error bars show the 95 % confidence interval of the distribution between the months on that day, as given in Eq. (6). The ensemble mean is always within the 95 % CI for both perturbed and unperturbed runs. **(b)** The dashed horizontal lines show the 95 % confidence internal of the ensemble, and the diamonds show each of the individual measurements on that day. The perturbed data are no more likely to fall outside this limit than the unperturbed data.

ACPD
12, 15373–15417, 2012

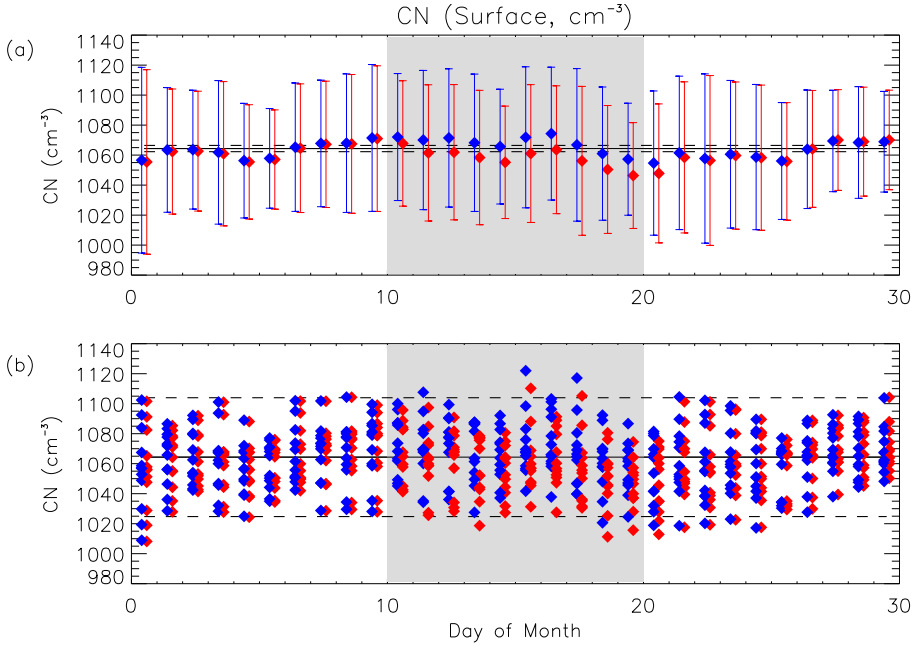

Fig. 5. Time series of surface-level CN_{10}. In both parts of each plot, the solid horizontal line shows the mean of all 360 measurements. Blue diamonds represent unperturbed values, and red diamonds represent perturbed values. **(a)** The dashed horizontal lines show the uncertainty on the mean, as given in Eq. (7). The diamonds show the daily means, and the error bars show the 95 % confidence interval of the distribution between the months on that day, as given in Eq. (6). The ensemble mean is always within the 95 % CI for both perturbed and unperturbed runs. **(b)** The dashed horizontal lines show the 95 % confidence internal of the ensemble, and the diamonds show each of the individual measurements on that day. The perturbed data are no more likely to fall outside this limit than the unperturbed data.

ACPD
12, 15373–15417, 2012

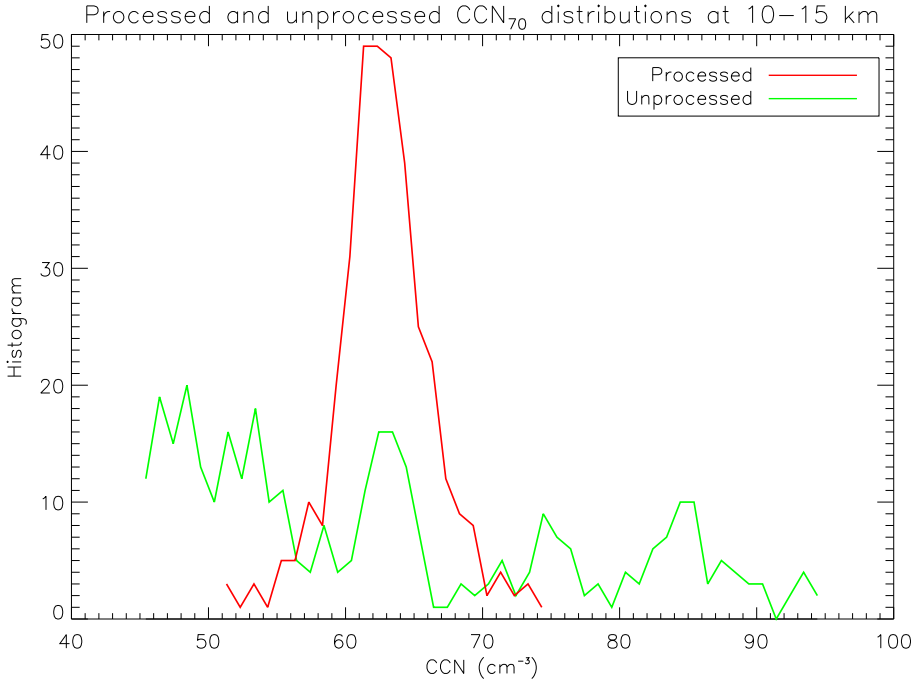

Fig. 6. Histograms showing the distribution of processed and unprocessed CCN_{70} concentrations at 10–15 km. The null hypothesis that the red line (processed) is normally distributed is rejected by the Lilliefors test.

ACPD
12, 15373–15417, 2012

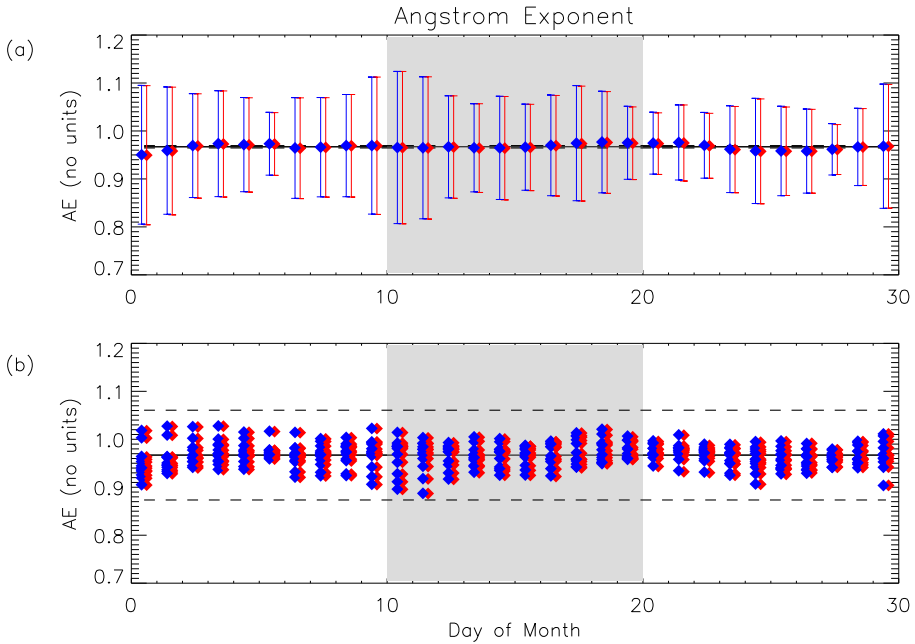

Fig. 7. Ångström exponent. In both parts of each plot, the solid horizontal line shows the mean of all 360 measurements. Blue diamonds represent unperturbed values, and red diamonds represent perturbed values. **(a)** The dashed horizontal lines show the uncertainty on the mean, as given in Eq. (7). The diamonds show the daily means, and the error bars show the 95 % confidence interval of the distribution between the months on that day, as given in Eq. (6). The ensemble mean is always within the 95 % CI for both perturbed and unperturbed runs. **(b)** The dashed horizontal lines show the 95 % confidence internal of the ensemble, and the diamonds show each of the individual measurements on that day. The perturbed data are no more likely to fall outside this limit than the unperturbed data.

ACPD
12, 15373–15417, 2012

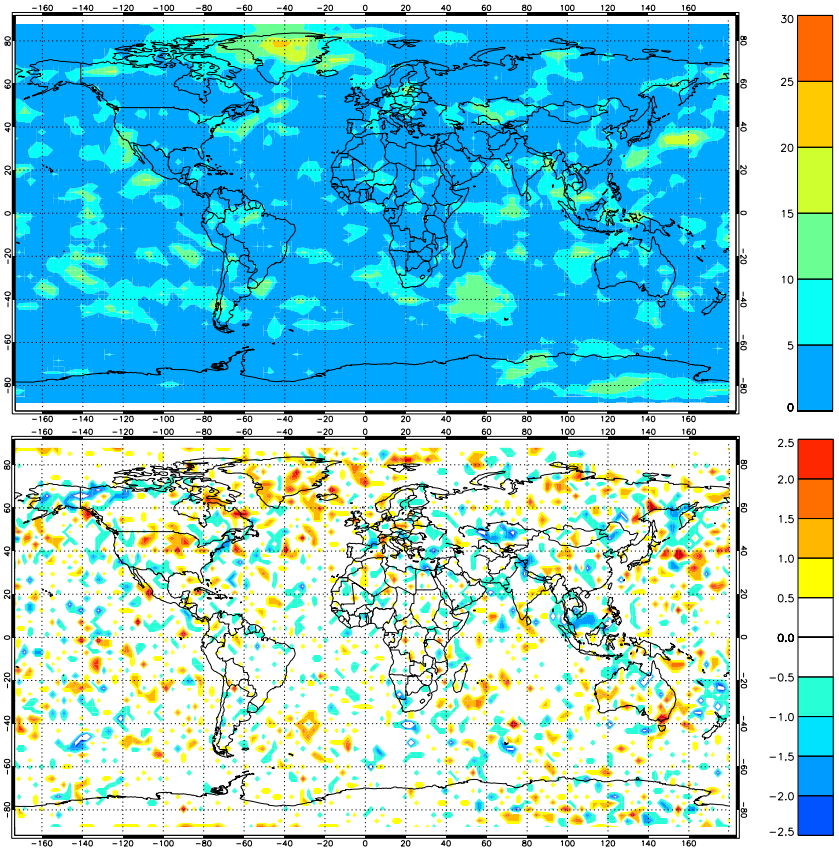

Fig. 8. A map showing regional values of **(a)** the number of model levels where $F > F_{\alpha}$, and **(b)** the difference between unperturbed and perturbed data, both in the case of surface CN_{10}.

ACPD
12, 15373–15417, 2012